# Geometrically Optimal Gaits for Passive-Elastic Inertial Swimmers

Nathan Justus* and Ross Hatton†
Collaborative Institude for Robotics and Intelligent Systems (CoRIS), Oregon State University
*justusn@oregonstate.edu †hattonr@oregonstate.edu

***Abstract*—A common movement strategy by animals and biomimetic robots is to locomote by interacting with the environment through cyclic shape changes, or gaits. Many animals make significant use of passive dynamics to reduce the effort required to execute these gaits. Although geometric tools have been developed to study passive gaits for swimmers in drag-dominated physics regimes, they have not yet been used to study larger-scale swimmers whose physics are dominated by inertial effects. In this paper, we leverage previous work in the geometric mechanics field to examine passive-elastic inertial swimmers, and show that geometric mechanics can be used to rapidly determine many classes of optimal gaits for such systems. In particular, we focus on three models of active-passive swimming inertial systems: the perfect-fluid Purcell swimmer, a swimmer with a continuously flexible passive 'fish' tail, and a symmetric breaststroke swimmer.**

***Index Terms*—Dynamics, Underactuated Robots, Nonholonomic Mechanisms and Systems**

## I. Introduction

A common movement strategy by animals and biomimetic robots is to locomote by interacting with the environment through cyclic shape changes, or *gaits*. The study of these motions is of interest, as it provides insight into the organisms that perform these gaits, and could lead to the development of biomimetic robots with improved maneuverability and increased mobility across different environmental terrains.

Animals often make use of passive-elastic elements to create beneficial characteristics in their gaits. Some fish, for example, have passive properties such that vorticity in a current can excite passive dynamics in the body and cause the fish to 'swim' upstream even after the fish has died [1]. Humans also take advantage of passive dynamics while walking: almost no muscle input is supplied to the leg during its swing phase [2].

The geometric mechanics community has developed a range of tools to study the properties of gaits for different locomotor physiologies. Many of these tools, however, assume that the locomotor shape space is fully actuated, and therefore cannot be directly applied to systems with passive body elements. Although previous works have developed geometric tools for the study of passive systems operating in drag-dominated regimes [3], many systems such as fish or other aquatic systems larger than a few millimeters in length operate outside of this regime. Such swimmers are better modelled as inertia-dominated systems swimming in a high Reynolds number 'perfect fluid' [4]. Although both low and high Reynolds number systems result in the similar overall geometric structures, perfect fluid swimmers require a different initial mathematical approach [5].

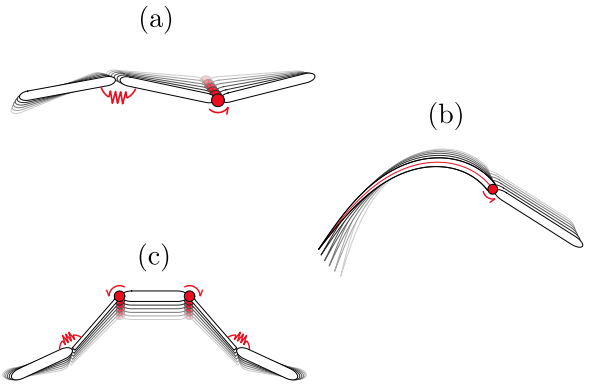


Fig. 1: Each of the active-passive swimmer models discussed in this paper, shown in motion due to gaits at their passive limit-cycles. Active joints are represented by red circle motors, and passive joints by red springs. (a) Purcell's swimmer (b) 'Fish' swimmer with a linear curvature passive tail (c) Symmetric 'breaststroke' swimmer

In this paper, we construct a framework for geometrically understanding the space of gaits in inertia-dominated systems with passive-elastic elements. We show that this framework produces compact equations of motion that enable rapid optimization of active-passive gaits. In particular, we will discuss three models of simulated active-passive systems, which are assumed to be swimming in a perfect fluid and are illustrated in Fig. 1:

(a) The perfect-fluid Purcell swimmer, with one passive joint
(b) A swimmer with a passive flexible curling tail
(c) A symmetric five-link 'breaststroke' swimmer

## II. Mathematical Formulation

In this section, we review the assumptions and techniques that facilitate this work, and provide the formulation for the optimization used in our following dynamic system examples. We then briefly discuss techniques for qualitatively understanding properties of optimal gaits.

### A. Obtaining the Equations of Motion

The models we employ in this paper are built upon the assumption that the system physics lie in the kinematic regime, where cessation of body shape changes results in a rapid return to zero body velocity with respect to the surrounding fluid [6]. In these models, it is assumed that fluid flow is directly coupled to link motion. This assumption allows for the formulation of body motion as a function of a system's shape variables $r$ and their time rate of change $\dot{r}$ through the momentum-free *reconstruction equation*,

$$\mathring{g} = \mathbf{A}(r)\dot{r}, \tag{1}$$

in which $\mathring{g}$ represents swimmer velocity expressed in its local body frame and $\mathbf{A}$ is the *motility map*, which linearly maps shape velocities to the resulting body velocities produced through fluid interaction.[1] The velocity $\mathring{g}$ in the swimmer's local frame can be converted into world-frame velocity $\dot{g}$ by rotating $\mathring{g}$ through the angle $\theta$, where $\theta$ is the orientation of the swimmer's local frame with respect to the world frame:

$$\dot{g} = \begin{bmatrix} \dot{x} \\ \dot{y} \\ \dot{\theta} \end{bmatrix} = R(\theta)\mathring{g} = R(\theta)\mathbf{A}(r)\dot{r}. \tag{2}$$

For inertial systems, the motility map can be found by first computing the total mass matrix. The total mass matrix is formulated by summing individual link fluid mass matrices $\mu_i$ pulled back through the link Jacobians $J_i$ relating swimmer velocity and shape velocity to link velocity in the link's frame:

$$M(r) = \begin{bmatrix} M_{gg} & M_{gr} \\ M_{rg} & M_{rr} \end{bmatrix} = \sum_i \left( J_i^T \mu_i J_i \right). \tag{3}$$

For inertial swimming systems, the individual link fluid mass matrices take into account both swimmer mass and added-mass effects (represented with the subscript $a$) coming from hydrodynamic interaction with the surrounding fluid:

$$\mu_i = \begin{bmatrix} m_{xy,i} + m_{ax,i} & 0 & 0 \\ 0 & m_{xy,i} + m_{ay,i} & 0 \\ 0 & 0 & m_{\theta,i} + m_{a\theta,i} \end{bmatrix} \tag{4}$$

Using (3), we can then compute the motility map [7]:

$$\mathbf{A}(r) = -M_{gg}^{-1} M_{gr}. \tag{5}$$

The total mass matrix can then be used to calculate the reduced mass matrix $M_r$, which is the swimmer's effective mass as represented in the swimmer shape space:

$$M_r(r) = \begin{bmatrix} \mathbf{A}^T(r) & I \end{bmatrix} M(r) \begin{bmatrix} \mathbf{A}(r) \\ I \end{bmatrix}. \tag{6}$$

Through Lagrangian analysis, the reduced mass matrix can be used to write the equations of motion for the systems shape variables given shape-space forces $\tau$ and Coriolis forces $C$ [5],

$$\tau = M_r(r)\ddot{r} + C(r, \dot{r}), \tag{7}$$

[1]In previous works, we have used the equation $\mathring{g} = -\mathbf{A}(r)\dot{r}$ and referred to $\mathbf{A}$ as the local connection. To reduce sign confusion, we have included the negative sign in $\mathbf{A}$ and chosen to refer to it as the motility map instead.

where the Coriolis forces can be calculated from derivatives of the reduced mass matrix as

$$C(r, \dot{r}) = \left( \sum_{i=1}^{d} \frac{\partial M_r(r)}{\partial r_i} \dot{r}_i \right) \dot{r} - \frac{1}{2} \begin{bmatrix} \dot{r}^T \frac{\partial M_r(r)}{\partial r_1} \dot{r} \\ \vdots \\ \dot{r}^T \frac{\partial M_r(r)}{\partial r_d} \dot{r} \end{bmatrix}. \tag{8}$$

### B. Optimizing with Passive Dynamics

By separating the shape space into actively controlled shape modes $r_c$ and passive shape modes $r_p$, the equation of motion for the passive joints can be written from (7) as

$$\tau_p = M_{cp}(r)\ddot{r}_c + M_{pp}(r)\ddot{r}_p + C_p(\dot{r}, r), \tag{9}$$

where $M_{pp}$ and $M_{cp}$ are blocks of the reduced mass matrix $M_r$ that correspond respectively to passive-mode masses and passive-active coupling masses. The quantity $\tau_p$ represents forces due to passive-elastic components acting on the passive shape modes. For a typical linear spring with positive constant $k$ and damper with positive constant $b$ acting on the passive joint, the generalized passive forces are

$$\tau_p = -kr_p - b\dot{r}_p. \tag{10}$$

For the case where the active shape modes are position controlled, the accelerations of the active modes in the shape space can be precalculated and the accelerations of the passive joints are found by solving (9) for $\ddot{r}_p$. For the case where the inputs to the active joints are forces and all accelerations are unknown, accelerations for both the active and passive joints can be solved together by composing $\tau$ as a vector of both active and passive shape forces and solving (7) for $\ddot{r}$.

In order to simulate these dynamics, we write the active joint control signal as a fourth-order Fourier function of time parameterized by the Fourier variables $a_{0-4}$, $b_{1-4}$, and $\omega$:

$$r_c(t) = a_0 + \sum_{i=1}^{4} \left( a_i \cos(i\omega t) + b_i \sin(i\omega t) \right). \tag{11}$$

By taking time derivatives of this equation, the joint velocities $\dot{r}_c$ and joint accelerations $\ddot{r}_c$ can be readily calculated. These values are used in (9) to numerically solve for the configurations of the passive modes over time.[2]

In order to obtain the dynamic limit cycle, we perform the simulations over three time-periods $T = \omega/2\pi$ for the gait, with the assumption that the passive modes will have stabilized to their final limit cycle by the end of the second period due to damping. The third period was used to calculate the total displacement of the swimming system as in (2),

$$g = \int_{2T}^{3T} R(\theta(t))\mathbf{A}(r(t))\dot{r}(t)dt. \tag{12}$$

[2]Our previous work [3] with viscous systems used Laplace transforms and frequency-space analysis to estimate the passive joint limit cycles, but unfortunately the technique is not suitable for inertia-dominated swimmers. The ODE in (7) is sufficiently nonlinear that the linearity assumptions required for limit-cycle estimation through frequency domain analysis are no longer valid, because the reduced mass matrix $M_r$ is heavily dependent on $r$.

Spatial displacement is found from the total displacement by taking the norm of the translation values:

$$D = \sqrt{g_x^2 + g_y^2}. \tag{13}$$

The limit-cycle values are also used to calculate the squared actuator-force cost for the active joint over the gait period, which has been previously used as a general-purpose model of actuator effort [5]:

$$E_\tau = \int_{2T}^{3T} \tau_c(t)^2 dt. \tag{14}$$

Two useful objective functions can be constructed from these values. The first is the speed efficiency $\eta_v = D/T$ which gives a measure of how far the swimmer will travel using a certain gait in unit time. The second is the energetic efficiency $\eta_\tau = D/E_\tau$, which gives a measure of how far the swimmer will travel per unit power consumption in the active joint.

By varying the Fourier parameters used to compute the position of the active joint over time in (11), these objective functions can be maximized, producing maximum-speed gaits and optimally energetically efficient gaits for any active-passive swimming system. In §III-§V, we examine the gaits resulting from this optimization process for each of the three systems proposed in this paper.

### C. The Constraint Curvature Function

Although the framework developed in the previous subsections allows for direct optimization of system behavior, it does not give insight into why optimization parameters might converge to a particular configuration. One useful tool that can grant such insight is the *constraint curvature function* (CCF). To introduce the CCF, we first recognize that the displacement of the swimmers due to a certain gait can be found as the line integral of the motility map over the system's limit cycle path $\phi$ through shape space

$$g = \oint_\phi R(\theta)\mathbf{A}(r). \tag{15}$$

In a manner similar to Stokes' theorem, this line integral can be approximated by a surface integral of the total Lie Bracket over the area enclosed by the gait $\phi_a$ [8]

$$g \approx \iint_{\phi_a} D\mathbf{A} = \iint_{\phi_a} d\mathbf{A} - [\mathbf{A}_1, \mathbf{A}_2], \tag{16}$$

where $d\mathbf{A}$ represents the generalized row-wise curl of the mobility map, finding net forwards minus backwards motion, and $[\mathbf{A}_1, \mathbf{A}_2]$ is a local Lie bracket term that corrects for non-commutativity as the swimmer translates and rotates through space. For planar translation and rotation for a system with two shape variables, the local Lie bracket is calculated as

$$[\mathbf{A}_1, \mathbf{A}_2] = \begin{bmatrix} \mathbf{A}_1^y \mathbf{A}_2^\theta - \mathbf{A}_2^y \mathbf{A}_1^\theta \\ \mathbf{A}_2^x \mathbf{A}_1^\theta - \mathbf{A}_1^x \mathbf{A}_2^\theta \\ 0 \end{bmatrix}. \tag{17}$$

The local Lie bracket is only a first order correction, and leaves remaining error that will scale with the size of the gait through shape-space. However, intelligent choice of the swimmer body frame can minimize the error of this approximation such that it can be neglected. For the systems discussed in this paper, useful coordinate frames are located approximately at the swimmer's center of mass and aligned with the principal moments of inertia. A general algorithm for calculating best body coordinates can be found in [9].

The total Lie bracket $D\mathbf{A}$ is a vector-valued function defined over the shape space. Each component of the vector is associated with a translational or rotational direction. The magnitude of that component represents how much enclosing that portion of shape space with the gait will contribute towards net motion of the swimmer in the associated direction. Components of the total Lie bracket associated with a single movement direction form the CCFs over the shape space.

The CCFs provide useful intuition as to what makes a 'good' gait for moving in a particular direction. The CCF for the Purcell swimmer in the X-direction is shown in Fig. 3. Gaits centered about the origin are more effective at achieving net x-displacement if they enclose primarily the positive black region in the center while minimizing the amount they enclose the surrounding negative red regions. Because a different convention was used in this paper for ordering joints, the sign of the CCF is reversed with respect to previous works. However, this convention change also reverses the chirality of gaits on the CCF, and so understanding gait properties is done through a qualitatively identical process.

It is worthy noting here that the inclusion of passive dynamics in the swimming systems does not change the CCF, which is completely determined by swimmer geometry: instead, passive dynamics place limitations on the allowable motions that can be drawn in the shape-space. For an ideal fully active system, gaits of arbitrary shape can be drawn. However, passive-elastic systems are underactuated and motion along the axis of the passive shape mode can only be indirectly controlled through motion of the active mode.

## III. The Purcell Swimmer

The Purcell swimmer was originally proposed as the simplest system capable of locomoting at low Reynolds numbers [10]. By performing the geometric process detailed in the previous section, this system can be constructed as a perfect-fluid swimmer locomoting in an idealized high Reynolds number environment. As illustrated in Fig. 2, the swimmer is composed of a chain of three elongated links, and swimmer

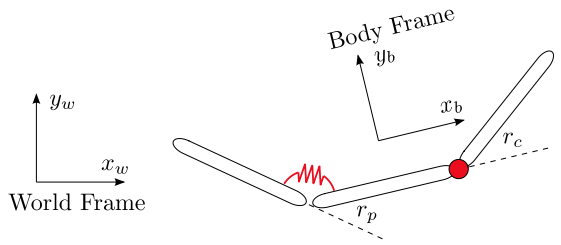


Fig. 2: Shape parametrization of the Purcell swimmer.

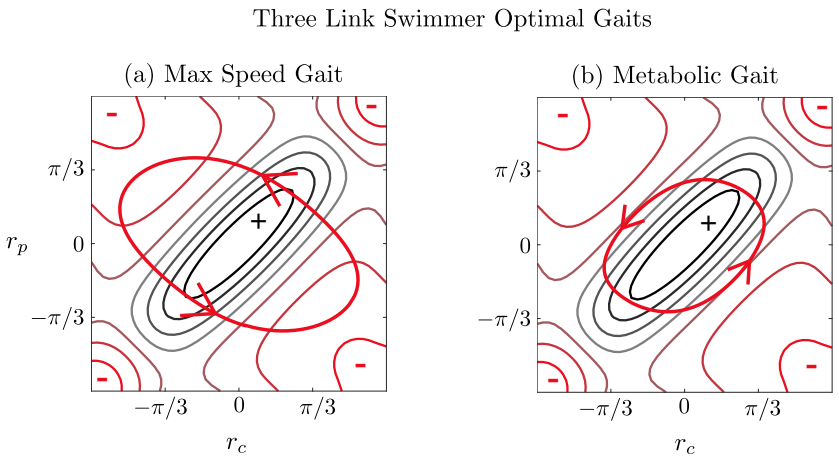


(c)

| Gait | Swimmer Speed (m/s) | Gait Period (s) | Max Motor Speed (rad/s) | Max Motor Torque (Nm) |
|---|---|---|---|---|
| Max Speed | 0.62 | 0.32 | 23.3 | 0.53 |
| Metabolic | 0.48 | 0.64 | 9.4 | 0.15 |

Fig. 3: Two locally optimal gaits for the active-passive Purcell swimmer superimposed on the X CCF: (a) the maximum-speed gait consisting of a simple sinusoid at the active link (b) a metabolic gait that compromises between the speed and efficiency using a metabolic scaling cost of $\gamma_m = 0.01$ (c) resulting speeds, gait periods, maximum actuator speeds, and maximum actuator torques for each gait, in the case of a 1-meter long Purcell swimmer. Optimal gaits tend to prioritize enclosure of the negative grey regions of the CCF while minimizing enclosure of positive red regions.

shape is parametrized by the angular deflection of the two joints in the chain.

Because of its relative simplicity, the Purcell swimmer is a useful system with which to characterize the general behavior of active-passive inertial swimmers. One notable quality of these passive inertial systems is their extreme nonlinearity. Because of this, it is difficult to optimize for design parameters such as spring and damping constants while also optimizing for gait parameters. However, the use of statistical optimization techniques such as simulated annealing that attempt to locate global rather than local maxima makes optimizations for both gait and design parameters possible [11]. For each of the swimmers discussed in this paper, a drag coefficient was chosen for the passive joint, and spring constants that enabled best movement were optimized simultaneously with motion parameters.

Results for optimizing swimmer speed are illustrated in Fig. 3(a) with numerical results shown in (c). The optimizer tends to converge toward simple sinusoidal gaits that operate at a frequency of approximately 3Hz for the 1-meter long Purcell swimmer with fluid density equal to that of the swimmer. For a damping constant of 0.01 Nms/rad, the optimal spring constant for these parameters converged to 0.074 Nm/rad. Unsurprisingly, the fastest possible gait for the Purcell swimmer requires rather high rotational speeds and torques from the actuator driving swimming motion, which are difficult hardware requirements. If the class of actuator being used to drive the active joint is known at the time of simulation, motion can be optimized so that hardware requirements are easily met.

Next we briefly discuss energetically efficient gaits found for the active-passive Purcell swimmer. Optimizing for energetically efficient gaits does not produce motions that would be feasible for physical swimmers. The optimizer finds that power consumption scales upwards much faster than locomotive distance for small gaits. This leads to convergence at gaits that produce very little actual displacement. For real-world swimmers, such miniscule gaits would produce motion that is dominated by fluid noise.

In general, optimizing the energetic efficiency of the swimmer is an attempt to minimize the amount of power consumed by the system that does not contribute to forward locomotion. For idealized systems, this is done by first prioritizing the reduction of system power consumption and taking advantage of passive locomotion. However, physical models of these systems will have sources of energy loss other than the actuator, such as processor power consumption. These baseline metabolic costs can be included into energetic efficiency by introducing a component that scales with the metabolic rate $\gamma_m$ and the gait time period $T$. This produces a new metabolic energy objective function:

$$\eta_m = \frac{D}{E_\tau + \gamma_m T}. \tag{18}$$

Results of optimizing with this new objective function intuitively scale with the baseline metabolic rate. When the swimmer metabolism is very low, optimizations converge towards low displacement gaits that prioritize reduction of actuator effort over actual locomotion. For swimmers with faster metabolisms, the time-scaling term dominates the energy

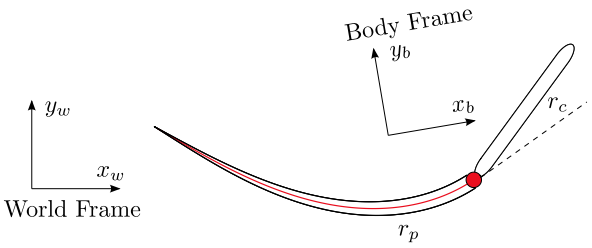


Fig. 4: Shape parametrization of the flexible-tail swimmer.

consumed by the active joint and the swimmer is encouraged to find speedy gaits. Such optimizations produce speed-optimal gaits like those shown in Fig. 3(a). Middling metabolism values, such as those calculated from processor power consumption, produce gaits that compromise between these two extremes. An example of such a metabolic gait is illustrated in Fig. 3(b). By optimizing for a metabolic rate $\gamma_m = 0.01$, we find a gait that is able to operate at approximately 75% of the optimal speed, while requiring less than half of the required motor speed and roughly a quarter of the required motor torque necessitated by the maximum-speed gait. Tuning the objective function to different metabolic rates allows for the optimization of gaits that lie along a Pareto frontier connecting optimal speed gaits to optimal energetically efficient gaits.

## IV. Flexible Tail Swimmer

Many locomotive mechanisms of interest to the robotics community [12], [13] utilize continuously flexible elements that do not bend at discrete joints. These systems are common in the study of aquatic locomotion, as many biological swimmers locomote using motions that continuously deform the body rather than with joint-like behavior.

The first step in optimizing gaits for a continuously flexible system is to identify the shape mode of passive body motions. For our model, we choose a linear-curvature bending mode for the passive 'tail', as illustrated in Fig. 4, with oscillations of an elongated 'head' driving locomotion. Curvature of the tail is at a maximum where it connects to the swimmer head, and decays linearly to zero at the tip of the tail in a manner reminiscent of biological fish motion. The tail is approximated by 21 links connected together in a chain. This produces 21 raw joints, 20 for the tail and one for the head. These joints can be reduced in dimensionality using active-passive modal reduction given a tail length $L_t$, number of tail joints $n$, and shape mode $\lambda_{\text{tail}}$:

$$r_{\text{raw}} = \lambda_{\text{tail}} r = \begin{bmatrix} L_t(1-1/n)/n & 0 \\ L_t(1-2/n)/n & 0 \\ \vdots & \vdots \\ L_t(1-n/n)/n & 0 \\ 0 & 1 \end{bmatrix} \begin{bmatrix} r_p \\ r_c \end{bmatrix}. \tag{19}$$

The shape mode provides a Jacobian mapping modal velocities to raw joint velocities, so modal reduction can be taken into account during mass matrix calculation in (3) to create the geometric system as a function of the desired shapes:

$$M(r) = \sum_i \left(\lambda^T J_i^T \mu_i J_i \lambda\right). \tag{20}$$

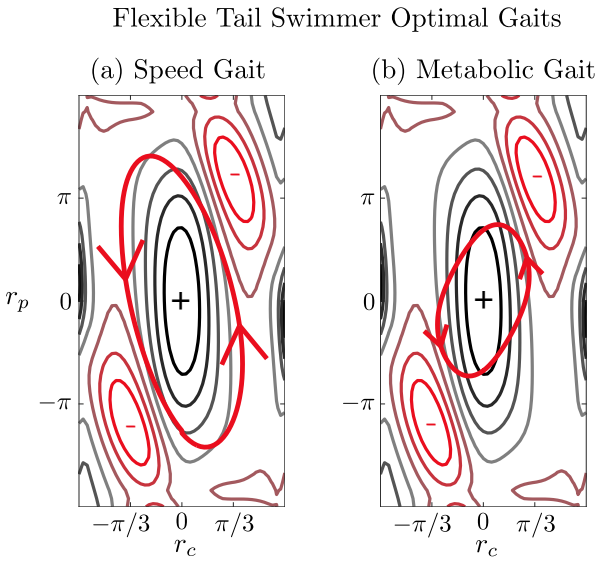


Fig. 5: Two locally optimal gaits for the flexible tail swimmer superimposed on the X-CCF: (a) the maximum speed gait, which operates at approximately 3Hz (b) a metabolic gait that compromises between speed and actuator effort

We choose the linear-curvature shape mode for its mathematical simplicity and mechanically intuitive nature, as it mirrors the deflection of a cantilever beam with a load applied at the tip. However, arbitrary shape modes can be used. If given motion data for points along a flexible body moving in fluid, appropriate shape modes can be extracted using the technique of eigenvector analysis [14]. This allows for the system to be simulated with behaviors that more closely resemble physical movements of the swimmers, leading to more accurate and useful gait analysis.

Similar to the Purcell swimmer, the flexible tail swimmer has different optimal gaits corresponding to each of the previously discussed objective functions. Speed-optimal gaits, as illustrated in Fig. 5(a), are formed with simple sinusoidal input into the active joint. By modifying the optimal-efficiency objective function with a metabolic cost, gaits such as the one illustrated in Fig. 5(b) are found that compromise between speed and power required by the head actuator.

## V. Breaststroke Swimmer

The final swimmer model that we will discuss in this paper is the symmetric breaststroke swimmer. Modelled after a humanlike system swimming through water, the system consists of five links chained together: two two-segment 'arms' are attached to a central body segment. Each arm consists of an upper arm segment that acts as a massless structural connection to the main body, and a lower arm segment that

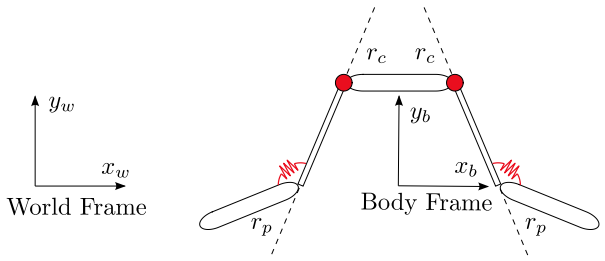


Fig. 6: Shape parametrization of the symmetric breaststroke swimmer.

acts as a paddle and provides propulsive force to the swimmer. The 'elbow' connection at the midpoint of the arm segments consists of a passive buckling spring with a different spring constant for each direction of deflection. Such anisotropic mechanisms have been shown to generate asymmetric gaits capable of producing net forward thrust for robotic swimmers by minimizing drag during the recovery stroke [15], and are a promising area of research for passive-inertial locomotors.

A diagram for the shape parametrization for the swimmer is illustrated in Fig. 6. The swimmer's configuration is symmetric about the central body, such that the shape can be described using only one passive mode and one active mode. The deflection of individual joints in order of appearance across the swimmer can be described the shape mode $\lambda_{\text{arms}}$

$$r_{\text{raw}} = \lambda_{\text{arms}} r = \begin{bmatrix} 1 & 0 \\ 0 & 1 \\ 0 & 1 \\ 1 & 0 \end{bmatrix} \begin{bmatrix} r_p \\ r_c \end{bmatrix}. \tag{21}$$

In a method identical to that of the flexible-tail swimmer discussed in the previous section, this shape mode can be included in the mass matrix calculation by (20) to reduce the system geometry to two dimensions.

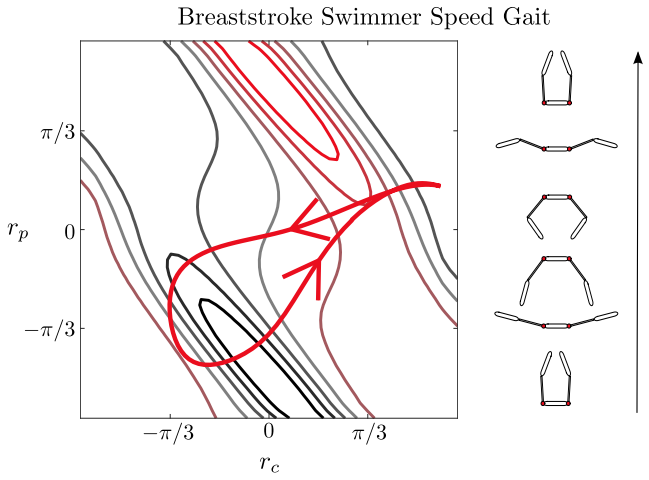


Fig. 7: Locally optimal speed gait for the breaststroke swimmer superimposed on the Y-CCF alongside images of swimmer shape along the gait

To represent the anisotropic buckling spring, we use a new equation for the torque on the passive joint where the spring constant is a function of the passive joint configuration

$$\tau_p = -k(r_p) r_p - b\dot{r}_p, \tag{22}$$

$$k(r_p) = \begin{cases} k_1, & r_p \leq 0 \\ k_2, & r_p > 0 \end{cases}. \tag{23}$$

By setting these spring constants to positive values and by imposing $k_2 > k_1$, beneficial anisotropic behavior emerges that generates breaststroke-like motion.

As shown in Fig. 7, the optimal speed gait makes heavy use of this asymmetry. As opposed to other swimming systems discussed in this paper, the high-value regions of the breaststroke swimmer's height function are not centered about the origin. The asymmetry of the passive joint mechanism allows for the region enclosed by the gait to shift away from the center and compensate for this in a way that avoids capturing oppositely-valued regions of the height function on the opposite side of the shape space.

## VI. Conclusion

In this paper, we showed that geometric mechanics provides a computationally simple framework for finding optimal gaits in inertial systems with passive elements. We believe that these tools can accelerate the design process for locomoting systems with passive dynamics by identifying promising families of motion, and that they provide fundamental intuition that can be useful for the development of such systems.

We discussed three models of inertial swimming systems with passive-elastic components. We used the passive Purcell swimmer as a simple model to introduce different families of optimal gaits that leverage passive dynamics to maximize swimmer speed. Next, we presented a flexible-tail swimmer to demonstrate how to geometrically represent continuously flexible systems, and showed that this flexible swimmer is qualitatively similar to the Purcell swimmer. Finally, we considered a symmetric breaststroke swimmer with anisotropic passive mechanisms at the joints and showed that passive asymmetry can allow for beneficial behavior in certain systems.

In future work, we will attempt to more realistically select passive shape-modes for continuously flexible elements. We will do this by comparing fluid forces exerted on the flexible element to constraint forces required to enforce the chosen shape-mode. We will also examine swimmer locomotion in non-perfect fluids that allow for fluid drag and attempt to find optimal gaits for geometric swimming systems with passive elements that can accrue momentum.

## VII. Acknowledgements

This work was supported by the NSF Emerging Frontiers in Research and Innovation (EFRI) program under award 1935324. We would also like to acknowledge Quinten Konyn for assistance in figure development.

## REFERENCES


[1] D. N. Beal, F. S. Hover, M. S. Triantafyllou, J. C. Liao, and G. V. Lauder, "Passive propulsion in vortex wakes," *Journal of Fluid Mechanics*, vol. 549, no. -1, p. 385, Feb. 2006. [Online]. Available: https://doi.org/10.1017/s0022112005007925

[2] T. McGeer, "Passive dynamic walking," *Int. J. Robotics Res.*, vol. 9, no. 2, pp. 62–82, 1990.

[3] S. Ramasamy and R. L. Hatton, "Optimal gaits for drag-dominated swimmers with passive elastic joints," *Physical Review E*, vol. 103, no. 3, p. 032605, 2021.

[4] E. Kanso, J. E. Marsden, C. W. Rowley, and J. B. Melli-Huber, "Locomotion of articulated bodies in a perfect fluid," *Journal of Nonlinear Science*, vol. 15, no. 4, pp. 255–289, 2005.

[5] R. L. Hatton, Z. Brock, S. Chen, H. Choset, H. Faraji, R. Fu, N. Justus, and S. Ramasamy, "The geometry of optimal gaits for inertia-dominated kinematic systems," 2021. [Online]. Available: https://arxiv.org/abs/2102.01506

[6] R. L. Hatton and H. Choset, "Geometric swimming at low and high reynolds numbers," *IEEE Transactions on Robotics*, vol. 29, no. 3, pp. 615–624, 2013.

[7] E. Kanso, J. E. Marsden, C. W. Rowley, and J. B. Melli-Huber, "Locomotion of articulated bodies in a perfect fluid," *Journal of Nonlinear Science*, vol. 15, no. 4, pp. 255–289, Aug. 2005. [Online]. Available: https://doi.org/10.1007/s00332-004-0650-9

[8] R. Hatton and H. Choset, "Nonconservativity and noncommutativity in locomotion," *The European Physical Journal Special Topics*, vol. 224, no. 17-18, pp. 3141–3174, Dec. 2015. [Online]. Available: https://doi.org/10.1140/epjst/e2015-50085-y

[9] R. L. Hatton and H. Choset, "Geometric motion planning: The local connection, stokes' theorem, and the importance of coordinate choice," *The International Journal of Robotics Research*, vol. 30, no. 8, pp. 988–1014, 2011.

[10] E. M. Purcell, "Life at low Reynolds number," *American journal of physics*, vol. 45, no. 1, pp. 3–11, 1977.

[11] D. Bertsimas and J. Tsitsiklis, "Simulated annealing," *Statistical Science*, vol. 8, no. 1, Feb. 1993. [Online]. Available: https://doi.org/10.1214/ss/1177011077

[12] J. Sánchez-Rodríguez, F. Celestini, C. Raufaste, and M. Argentina, "Proprioceptive mechanism for bioinspired fish swimming," *Physical Review Letters*, vol. 126, no. 23, Jun. 2021. [Online]. Available: https://doi.org/10.1103/physrevlett.126.234501

[13] G. V. Lauder, B. Flammang, and S. Alben, "Passive robotic models of propulsion by the bodies and caudal fins of fish," *Integrative and Comparative Biology*, vol. 52, no. 5, pp. 576–587, Jun. 2012. [Online]. Available: https://doi.org/10.1093/icb/ics096

[14] G. J. Stephens, B. Johnson-Kerner, W. Bialek, and W. S. Ryu, "Dimensionality and dynamics in the behavior of c. elegans," *PLoS Computational Biology*, vol. 4, no. 4, p. e1000028, Apr. 2008. [Online]. Available: https://doi.org/10.1371/journal.pcbi.1000028

[15] M. Sharifzadeh and D. M. Aukes, "Curvature-induced buckling for flapping-wing vehicles," *IEEE/ASME Transactions on Mechatronics*, vol. 26, no. 1, pp. 503–514, Feb. 2021. [Online]. Available: https://doi.org/10.1109/tmech.2020.3034659